Catalysis Today 148 (2009) 398–404

Contents lists available at ScienceDirect

Catalysis Today

journal homepage: www.elsevier.com/locate/cattod

Ruthenium and rhodium nanoparticles as catalytic precursors in supercritical carbon dioxide

Martha V. Escárcega-Bobadilla [a,b], Clara Tortosa [b], Emmanuelle Teuma [a], Christian Pradel [a], Aránzazu Orejón [b], Montserrat Gómez [a,*,1], Anna M. Masdeu-Bultó [b,*]

[a] Laboratoire Hétérochimie Fondamentale et Appliquée, UMR CNRS 5069, Université Paul Sabatier, 118, route de Narbonne, 31120 Toulouse Cedex 9, France
[b] Departament de Química Física i Inorgànica, Universitat Rovira i Virgili, Marcel lí Domingo s/n, 43007 Tarragona, Spain

ARTICLE INFO

Article history:
Available online 3 September 2009

Keywords:
Ruthenium
Rhodium
Nanoparticles
Supercritical carbon dioxide
Fluorinated phosphines
Catalytic hydrogenation

ABSTRACT

Ruthenium and rhodium nanoparticles (MNP) were prepared in the presence of phosphine ligands containing fluorinated groups, starting from well-defined organometallic compounds. The syntheses of these new materials evidenced the crucial tuning between metal precursor and ligand. These nanocatalysts were used in hydrogenation reactions of arene derivatives in organic solvent (THF) and supercritical carbon dioxide ($scCO_2$). The catalytic behaviour observed (activity and selectivity) showed that both Ru and Rh systems are less active in $scCO_2$ than in THF, preventing the hydrogenation of the aromatic group when electron-donor groups (like ether moieties) are present on the substrate.

1. Introduction

The recent developments in the field of metallic nanoparticles (MNP) have demonstrated that they are excellent catalytic materials for the hydrogenation of alkenes and arenes under mild conditions [1–5]. Selective hydrogenation is an efficient and widely applied synthetic procedure for industrial processes and syntheses of fine chemicals [6,7]. Hydrogenation of arenes to produce cyclohexanes is an important reaction, especially the hydrogenation of benzene, which is used for the industrial production of adipic acid, a precursor for the nylon manufacture [8]. This process is performed using heterogeneous catalysts, usually under drastic conditions.

Concerning nanocatalysts, hydrogenation reactions are mostly performed in organic solvents [9]. From an environmental point of view, advices to reduce the use of volatile organic compounds in all kind of processes are strongly encouraged [10]. One alternative for catalysed reactions is the use of supercritical carbon dioxide ($scCO_2$), considered as a *green* solvent [11]. Its low polarity and variable density with pressure and temperature, make it an appropriate medium for reactions involving a wide variety of organic reagents. In addition, $scCO_2$ shows a high miscibility with gases, rendering it particularly suitable for hydrogenation reactions [12,13], since hydrogen has limited solubility in organic solvents [14]. Furthermore, $scCO_2$ can easily gain access to the active centres in metal nanoparticles, due to its low viscosity and high diffusivity [15].

In the last years, the preparation of metal nanoparticles in supercritical fluids (SCF) has been developed [16–21]. Stabilisers such as dendritic polymers functionalized with perfluoroalkyl, perfluorooligoether, polysiloxane, non-fluorinated alkyl and oligoethylene glycol moieties have been used to prepare palladium and silver nanoparticles [19]. Silver nanocrystals ranging from 20 to 100 Å were prepared in $scCO_2$ using perfluorinated thiols [22,23]. In many examples, the nanoparticles are found stabilised by water-in-$scCO_2$ microemulsions [24–26].

MNP-catalysed hydrogenation processes in supercritical fluids, especially in $scCO_2$, are scarcer. Rh, Pd and Ru nanoparticles stabilised by surfactants in water/SCF mixtures [27,28] or in water-in-$scCO_2$ microemulsions are frequently used [24,29–31]. However, the aqueous surfactant solutions present important drawbacks, mainly the low solubility of organic substrates, besides the difficulty to control the pH under these conditions. A further original approach to prepare MNP in $scCO_2$ has been described taking advantage of the swelling of the plastics in $scCO_2$, which act as stabilisers of Rh and Pd nanoparticles applied in hydrogenation catalytic reactions [32].

In relation to the stabilisation of MNP, a great variety of stabilisers (surfactants, polymers, macromolecules, dendrons and

* Corresponding authors.
E-mail addresses: gomez@chimie.ups-tlse.fr (M. Gómez), annamaria.masdeu@urv.net (A.M. Masdeu-Bultó).
[1] Université de Toulouse, UPS, LHFA, 118 route de Narbonne, F-31062 Toulouse, France. Tel.: +33 5 61 55 77 38; fax: +33 5 61 55 82 04.

0920-5861/$ – see front matter © 2009 Elsevier B.V. All rights reserved.
doi:10.1016/j.cattod.2009.07.112

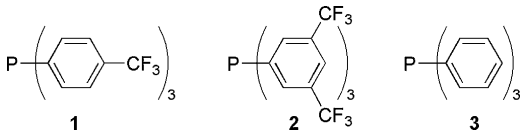

Fig. 1. P-donor ligands (**1**–**3**) used to stabilise **RhL** and **RuL** nanoparticles.

ligands) have been employed [33]. In particular, ligands become attractive as MNP stabilisers to be applied in catalysis, due to their coordination to the metallic surface allowing the selectivity induction in the catalytic reaction, analogously to the behaviour of classical homogeneous catalysts. While P-donor ligands have been extensively used in hydrogenation processes catalysed by organometallic complexes, few reports are related to their catalytic applications concerning MNP. Therefore, Fujihara and co-workers reported Binap-stabilised palladium nanoparticles (Binap = 2,2′-bis(diphenylphosphino)-1,1′-binaphtyl), which led to high enantiomeric excess (ee) in the asymmetric hydrosilylation of styrene under mild conditions (ee up to 95%) [34]. One of us also used chiral xylofuranide diphosphites to prepare PdNP, which were highly enantioselective in the allylic alkylation reactions (up to 97% of ee) [35,36].

Here, we report for the first time the preparation of rhodium and ruthenium nanoparticles stabilised by phosphines containing fluorinated groups (Fig. 1), with the aim to increase the affinity of MNP to $scCO_2$. The catalytic behaviour of these new materials in the hydrogenation of different arenes has been also evaluated in both organic (THF) and supercritical ($scCO_2$) solvents.

2. Experimental

2.1. General

MNP syntheses were performed using standard Schlenk techniques and Fisher–Porter bottle techniques under argon atmosphere. Organic solvents were dried following the procedures described in the literature [37]. Reagents and solvents were degassed by three vacuum–argon or vacuum–nitrogen cycles. Metallic nanoparticles were prepared by organometallic compound decomposition following the methodology described in the literature [38]. [Ru(cod)(cot)], 4-trifluoromethyltriphentlphosphine, 3,5-bistrifluoromethyl triphenylphosphine, triphenylphosphine, ruthenium 5% on activated carbon, styrene, 4-methyl anisole, dodecanethiol and fluorobenzene were purchased from Nanomeps, Alfa Aesar and Aldrich and used without further purification. $[Rh(\mu\text{-OMe})(cod)]_2$ [39,40] and 2-methylprop-2-enoxybenzene [41] were synthesized following the procedures described in the literature. Elemental analyses of Rh and Ru were carried out in a PerkinElmer Optima 3200 RL apparatus. Carbon and hydrogen analyses were done in a PerkinElmer 240 B apparatus. TEM and HR-TEM experiments were performed on a JEOL 200 CX-T electron microscope operating at 200 kV and a Philips CM12 electron microscope operating at 120 kV with respective resolutions of 4.5 and 5 Å. TEM analyses of the nanoparticles after catalysis were performed on a Zeiss 10 CA electron microscope at 100 kV with a resolution of 3 Å. Samples for TEM analysis were prepared by slow evaporation of a drop colloidal solution deposited under argon onto holey carbon-covered copper grids. Gas chromatography analyses (undecane used as an internal standard) were performed with a Hewlett-Packard 5890A instrument in an HP-5 (5% diphenylsilicone/95% dimethylsilicone column, 25 m × 0.2 mm), equipped with a Hewlett-Packard HP3396 series II integrator. Catalytic experiments in $scCO_2$ were performed in a Parr autoclave (25 mL) with magnetic stirring. The autoclave was equipped with a liquid inlet, a gas inlet, a CO_2 inlet and a thermocouple. An electric heating mantle kept the temperature constant. Catalytic experiments in organic solvent were carried out in a Berghof autoclave (125 mL) with magnetic stirring and capacity of 100 atm of pressure equipped with gas and liquid inlet. An electric heating mantle kept the temperature constant.

2.2. General synthesis of RuNP stabilised by phosphine ligands (*Ru2 and Ru3*)

In a typical experiment, 0.016 mmol of the appropriate ligand was introduced in a Fisher–Porter bottle and left under vacuum during 30 min. A solution of 25 mg of [Ru(COD)(COT)] (0.08 mmol) in 5 mL of neat THF, deoxygenated by freeze-pump cycles, was then added; and a total volume of 80 mL of THF was achieved. The bottle was then pressurized under 3 bar of H_2 pressure and stirred vigorously. After 18 h, a homogeneously brown solution was obtained and depressurized. Solvent was evaporated under vacuum up to approximately 10 mL. Deoxygenated pentane (10 mL) was then added and a brown precipitate was formed. After filtration, the precipitate was washed with deoxygenated pentane (2 × 10 mL) and dried under reduced pressure. The resulting black powder obtained was characterized by IR spectroscopy, TEM and elemental analysis; **Ru2** was also analysed by powder XRD.

Ru2. Mass: 19.6 mg. IR (KBr pellet): 798 (C–P st, w), 1063 (C–F st, w), 423 (Ru–P) cm^{-1}. Elemental analysis: Ru = 19.73%, C = 45.36%, H = 7.16%. Calculated for Ru_5(**2**)$(THF)_{20}$: Ru = 19.3%, C = 47.7%; H = 6.5%. Mean diameter (TEM) = 1.3 ± 0.27 nm (111 particles). XRD: hcp.

Ru3. Mass: 21.4 mg. IR (KBr pellet): 804 (C–P st, w), 500 (Ru–P) cm^{-1}. Elemental analysis: Ru = 16.6%, C = 51.45%, H = 8.46%. Calculated for Ru_5(**3**)$(THF)_{30}$: Ru = 17.3%, C = 56.6%; H = 8.7%. Mean diameter (TEM) = 1.38 ± 0.43 nm (792 particles).

2.3. General synthesis of RhNP stabilised by phosphine ligands (*Rh1 and Rh3*)

In a typical experiment, 3.87 mg of $[Rh(\mu\text{-OMe})(COD)]_2$ (0.008 mmol) and 0.0032 mmol of the appropriate ligand were introduced in a Fisher–Porter bottle and left under vacuum during 30 min. 80 mL of neat THF, deoxygenated by freeze-pump cycles, was then added. The bottle was pressurized under 3 bar of hydrogen and stirred vigorously. After 18 h, a homogeneous grey solution was obtained and depressurized. Solvent was evaporated under vacuum up to approximately 10 mL. Deoxygenated pentane (10 mL) was then added and a black precipitate was formed. After filtration, the precipitate was washed with deoxygenated pentane (2 × 10 mL) and dried under reduced pressure. The resulting black powder obtained was characterized by IR spectroscopy, TEM and elemental analysis.

Rh1. Mass: 3.1 mg. IR (KBr pellet): 802 (C–P st, w), 1261 (C–F st, w) cm^{-1}. Elemental analysis: Rh = 27.1%, C = 47.72%, H = 6.61%. Calculated for Rh_5(**1**)$(THF)_{15}$: Rh = 25.0%, C = 47.2%; H = 6.4%. Mean diameter (TEM) = 2.51 ± 0.42 nm.

Rh3. Mass: 3.3 mg. IR (KBr pellet): 802 (C–P st, w) cm^{-1}. Elemental analysis: Rh = 17.2%, C = 56.26%, H = 7.73%. Calculated for Rh_5(**3**)$(THF)_{30}$: Rh = 17.5%, C = 56.4%; H = 8.7%. Mean diameter (TEM) = 1.73 ± 0.46 nm.

2.4. Ligand exchange reaction monitored by NMR

10 mg of **Ru2** nanoparticles, 0.7 mL of THF-d_8 and 0.03 mL (0.3 mmol) of fluorobenzene as an internal standard were introduced in a NMR Young joint tube. After ^{19}F and ^{31}P NMR spectra recording, 0.1 mL of dodecanethiol (0.4 mol) was added

and the tube was gently stirred to homogenate the solution. ^{19}F and ^{31}P NMR spectra were recorded on time.

2.5. Hydrogenation reactions using MNP as catalytic precursors in THF

As a general procedure for preformed MNP as a catalytic precursor, 0.009 mmol of MNP was then introduced in the Berghof autoclave in a glove box to ensure the inert atmosphere inside. 4.5 mmol of substrate and 20 mL of neat and deoxygenated THF were then added. The autoclave was pressurized at 20 atm of H_2, stirred and heated at 50 °C during 24 h. After cooling to 0 °C, the autoclave was depressurized and the reaction mixture was then filtered through a celite column.

2.6. Hydrogenation of arenes with metallic nanoparticles in $scCO_2$

As a general procedure for preformed MNP as a catalytic precursor, 0.011 mmol of MNP was introduced in the Parr autoclave in a glove box to ensure the inert atmosphere inside. 5.6 mmol of substrate was then added. The autoclave was pressurized at 20 atm of H_2 and pressurized with CO_2 at 200 atm of total pressure. The autoclave was stirred and heated at 50 °C during 24 h. The autoclave was then cooled at 0 °C and slowly depressurized through a cold trap. The reaction mixture was extracted with diethylether and the reaction mixture was then filtered through a celite column.

3. Results and discussion

3.1. Synthesis of rhodium and ruthenium nanoparticles

Metallic nanoparticles were prepared by decomposition of organometallic precursors under reductive atmosphere following the general methodology elsewhere described [42]. Therefore $[Rh(\mu\text{-OMe})(cod)]_2$ or [Ru(cod)(cot)] (cod = 1,5-cyclooctadiene; cot = cyclooctatriene) dissolved in THF in the presence of a phosphine (**1–3**, Fig. 1) were pressurized under hydrogen at room

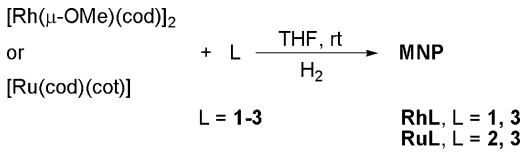

Scheme 1. Synthesis of Rh and Ru nanoparticles stabilised by ligands **1**–**3** (cod = 1,5-cyclooctadiene; cot = cyclooctatriene).

temperature (Scheme 1). MNP were precipitated with pentane giving black solids. Triphenylphosphine acted as a good stabiliser for both metals (**Rh3** and **Ru3**), while the fluorinated phosphines **1** and **2** behaved differently depending on the metal nature, leading to the formation of rhodium **Rh1** (but not **Rh2**) and ruthenium **Ru2** (but not **Ru1**) nanoparticles. This behaviour could be related to the relative size of the nanoclusters (rhodium nanoparticles, bigger than ruthenium ones, see Table 1) and, in consequence, to the relative ratio of coordination sites (placed on vertexes, edges or faces), showing a preference for the less-sterically demanding ligand (**1**) when bigger rhodium particles are involved, even though its lower Lewis basicity compared with ligand **2**. It is important to note that RuNP were isolated starting from relative high metal concentration (10^{-3} mol L^{-1}), however RhNP were obtained working at more diluted conditions ([Rh] $\leq$ 10^{-4} mol L^{-1}), otherwise agglomerates were only observed. Concerning the metal/ligand ratio (M/L), the syntheses were reproducible at ratios $\geq$1/0.2 (up to 1/1).

Metal nanoparticles were analysed by TEM (Figs. 2 and 3). The micrographs corresponding to RuNP, **Ru2** and **Ru3** (Fig. 2), showed the formation of small nanoparticles (ca. mean diameter of 1.3 nm), reasonably homogenous in size and well-dispersed on the grid (Fig. 2). In contrast, rhodium nanoparticles were bigger, exhibiting a tendency to agglomerate. In addition, the ligand nature induced significant size differences in the case of Rh nanoparticles (Fig. 3), being smaller (ca. 1.7 nm) and less dispersed in size with triphenylphosphine as a stabiliser than with the fluorinated phosphine **1** (ca. 2.5 nm), while for RuNP no differences were observed. The powder XRD analysis of **Ru2** showed the

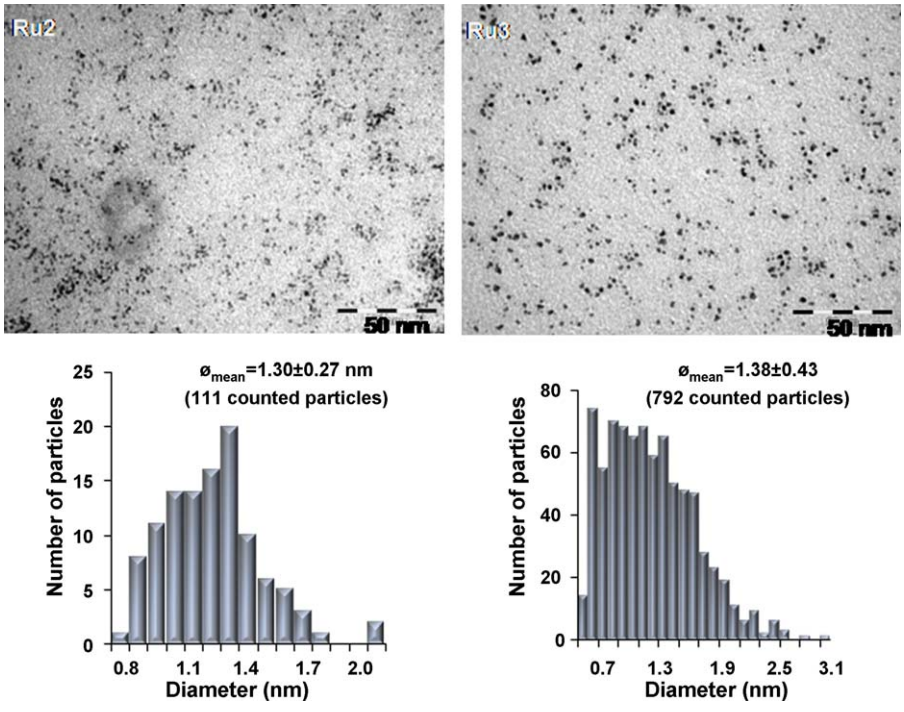

Fig. 2. TEM micrographs of **Ru2** (left) and **Ru3** (right) with the corresponding size distribution diagram.

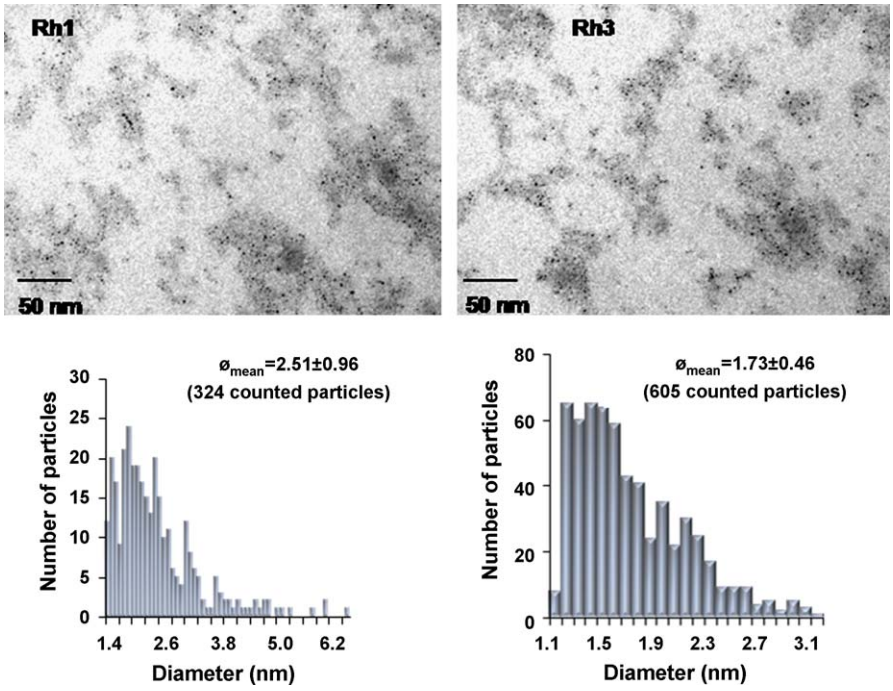

Fig. 3. TEM micrographs of **Rh1** (left) and **Rh3** (right) with the corresponding size distribution diagram.

hexagonal cubic packing of the metallic core, analogously to that of bulk metal (see Figure S1 in the Supplementary material). Infrared spectra (recorded range: 4000–400 cm^{-1}) of these materials analysed as KBr pellets, evidenced the presence of the phosphine ligands and the absence of their oxide partners (no absorption bands at ca. 1300 cm^{-1} were observed in any case, see Figure S2 in the Supplementary material). The high energy shift observed for the C–P stretching absorption band for MNP (in the range of 798–804 cm^{-1}) compared to that corresponding to the free ligands (701–745 cm^{-1}), points to a M(0)–P back-donation strengthening the C–P bond. This electronic density increase on the phosphine also induces an effect on the C–F stretching of the trifluoromethyl groups; actually, C–F bond reinforces when placed at *para* position in relation to the phosphorous atom (**Rh1**: 1261 cm^{-1} versus 1164 cm^{-1}) and weakens when placed at *meta* position (**Ru2**: 1063 cm^{-1} versus 1131 cm^{-1}). Raman spectra for RuNP allowed the Ru–P stretching assignment (see Table 1).

In order to check the stability of the ligand under the reductive synthesis conditions, we carried out an exchange ligand reaction between **Ru2** nanoparticles and dodecanethiol using fluorobenzene as an internal standard. The reaction was monitored by ^{19}F (Fig. 4) and ^{31}P NMR (Figure S3 in Supplementary material). After 22 days, the phosphine displacement was estimated in 56%, without any sign of phosphine hydrogenation.

3.2. Catalytic reactivity of rhodium and ruthenium nanoparticles

Preformed MNP (**Rh1**, **Rh3**, **Ru2** and **Ru3**) were used as catalytic precursors for the hydrogenation reaction of styrene (**4**) and p-methylanisole (**5**) in THF and in $scCO_2$ (Scheme 2).

The rhodium systems were able to hydrogenate the substrate **4**, leading to a total styrene conversion in both solvents (entries 1–4, Table 2). But only in THF the product corresponds to the full hydrogenated compound (**4a**), while in $scCO_2$ medium, the major product corresponds to ethylbenzene (**4b**) (entries 1 and 3 versus 2 and 4, respectively, Table 2). On the contrary, **Rh1** and **Rh3** were inactive for the p-methylanisole hydrogenation in both solvents (entries 5–8, Table 2), being **Rh1** somewhat active in $scCO_2$ (entry 6, Table 2), favouring the fully hydrogenated product (**5a**).

Better activities were obtained for substrates **4** and **5** in both solvents using Ru nanocatalysts (entries 10–16, Table 2), than those observed for Rh catalysts, favouring in all the cases the formation of the full hydrogenated product. It is important to note that **Ru2** and **Ru3** were less active for p-methylanisole than for styrene (entries 9–12 versus 13–16, Table 2), trend also observed for rhodium based catalysts.

TEM micrographs after styrene hydrogenation in $scCO_2$ showed that Ru nanoparticles were well-dispersed, in contrast to those reactions carried out in THF (Fig. 5). However, using rhodium

Table 1
Diameter and IR data for MNP (**Rh1**, **Rh3**, **Ru2** and **Ru3**).

MNP	*d* (nm)[a]	IR data (cm^{-1})[b]	Calculated formula from elemental analysis[c]
Rh1	2.51 ± 0.96 (Rh_{595})	802(C–P st, w), 1261 (C–F st, w) [701 (C–P st, w), 1164 (C–F st, w)][d]	Rh_5(**1**)$(THF)_{15}$ (Rh_{595}(**1**)$_{119}(THF)_{1785}$)
Rh3	1.73 ± 0.46 (Rh_{195})	802 (C–P st, w) [745 (C–P st, w)][d]	Rh_5(**3**)$(THF)_{30}$ (Rh_{195}(**3**)$_{39}(THF)_{1170}$)
Ru2	1.30 ± 0.27 (Ru_{85})	798 (C–P st, w), 1063 (C–F st, w), 423 (Ru–P)[e] [704 (C–P st, w), 1131 (C–F st, w)][d]	Ru_5(**2**)$(THF)_{20}$ (Ru_{85}(**2**)$_{17}(THF)_{340}$)
Ru3	1.38 ± 0.43 (Ru_{101})	804 (C–P st, w), 500 (Ru–P)[e] [745 (C–P st, w)][d]	Ru_5(**3**)$(THF)_{30}$ (Ru_{101}(**2**)$_{20}(THF)_{606}$)

[a] Determined by TEM. In brackets, the estimated metallic composition considering a compact packing arrangement of spherical nanoparticles (hcp for Ru and fcc for Rh clusters).
[b] Data in the range of 4000–400 cm^{-1}; samples prepared as KBr pellets; in brackets, the attribution and relative intensity of the bands.
[c] In brackets, the proposed formula on the basis of the metallic nanocluster composition.
[d] In square brackets, the corresponding IR data for the appropriated free ligand.
[e] Frequencies observed by Raman spectroscopy (range recorded: 4000–200 cm^{-1})

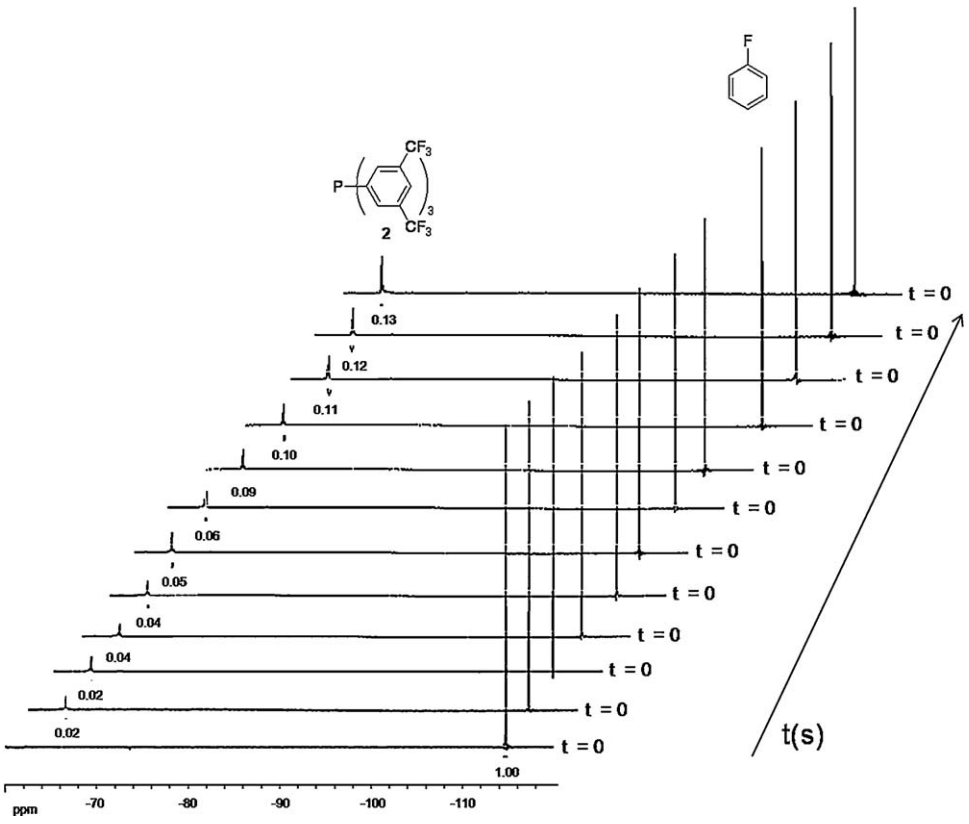

Fig. 4. ^{19}F NMR monitoring (THF-d_8, 298 K, 376.1 MHz) corresponding to the exchange reaction of **Ru2** nanoparticles with dodecanethiol.

nanoparticles, agglomeration was observed in both solvents, fact probably related to the lower activity of these systems in relation to those based on ruthenium due to a relative decrease of the metallic surface [9].

In order to avoid the steric hindrance induced by the methyl group on the substrate **5** and to study the selectivity between an aromatic ring and a double bond, we tested the hydrogenation of **6** using the most active systems, **Ru2** and **Ru3**. In THF, the systems were moderately active (up to 44% conversion, entries 17 and 19, Table 2), obtaining essentially the product corresponding to the hydrogenation of the exocyclic double bond (**6a**). Analogously to the behaviour observed for **5**, both catalytic systems were less active in $scCO_2$ (up to 23% substrate conversion, entries 18 and 20, Table 2); in addition, **Ru3** in $scCO_2$ favoured the isomerisation reaction (**6a**/**6b** = 63/37). When Ru/C was used as a catalyst, lower activities were found than those obtained with the corresponding nanoparticle-based catalysts for the substrates **4** and **5** (for **4**, entries 9 and 11 versus 21; for **5**, entries 13 and 15 versus 22, Table 2); but no significant differences were observed for **6** (entries 17 and 19 versus 23, Table 2). These results point to a strong interaction between the aromatic and the metallic surface of the nanoparticles, mainly for **4** and **5**, in agreement with the NMR

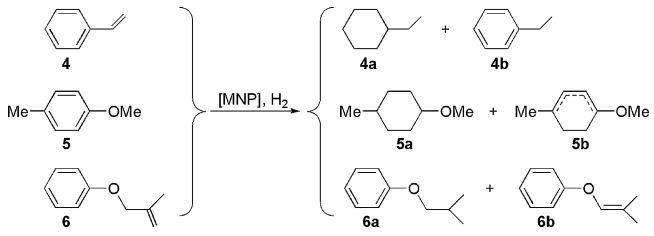

Scheme 2. Ruthenium- and rhodium-catalysed hydrogenation reactions.

Table 2
Metal-catalysed hydrogenation of substrates **4**–**6** using preformed MNP (**Rh1**, **Rh3**, **Ru2** and **Ru3**) as catalytic precursors (see Schemes 1 and 2).[a]

Entry	Catalytic precursor	Substrate	Solvent	Conv. (%)[b]	Selectivity[c]
1	**Rh1**	**4**	THF	100	100:0
2	**Rh1**	**4**	$scCO_2$	100	40:60
3	**Rh3**	**4**	THF	100	99:1
4	**Rh3**	**4**	$scCO_2$	100	30:70
5	**Rh1**	**5**	THF	0	–
6	**Rh1**	**5**	$scCO_2$	21	85:15
7	**Rh3**	**5**	THF	4	nd
8	**Rh3**	**5**	$scCO_2$	0	–
9	**Ru2**	**4**	THF	100	100:0
10	**Ru2**	**4**	$scCO_2$	100	100:0
11	**Ru3**	**4**	THF	100	78:22
12	**Ru3**	**4**	$scCO_2$	100	100:0
13	**Ru2**	**5**	THF	100	100:0
14	**Ru2**	**5**	$scCO_2$	52	91:9
15	**Ru3**	**5**	THF	73	98:2
16	**Ru3**	**5**	$scCO_2$	24	94:6
17	**Ru2**	**6**	THF	44	90:10
18	**Ru2**	**6**	$scCO_2$	18	92:8
19	**Ru3**	**6**	THF	41	96:4
20	**Ru3**	**6**	$scCO_2$	23	63:37
21	**Ru/C**[d]	**4**	THF	100	0:100
22	**Ru/C**[d]	**5**	THF	10	80:20
23	**Ru/C**[d]	**6**	THF	96	90:10

[a] *Catalytic conditions*: $T = 50\,^{\circ}C$; $t = 24$ h; M_{total}: $S = 1{:}500$; $[M] = 4.5 \times 10^{-4}$ M; gas pressure: in THF: $P_{H_2} = 20$ bar; in $scCO_2$: $P_{H_2} = 20$ bar, $P_{total} = 200$ bar. Results from duplicate experiments.
[b] Determined by GC.
[c] Determined by GC–MS. For substrate **4**, the ratio corresponds to **4a**:**4b**; for **5**, **5a**:**5b** and for **6**, **6a**:**6b**.
[d] Ru, 5% on activated carbon.

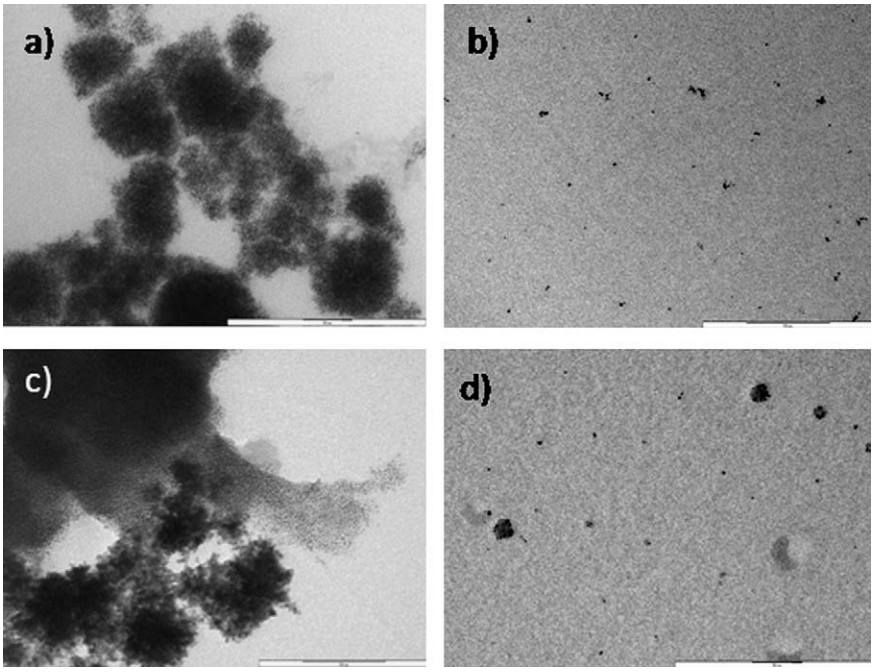

Fig. 5. TEM micrographs of RuNP after styrene hydrogenation. Top: **Ru2** in (a) THF and (b) $scCO_2$. Bottom: **Ru3** in (c) THF and (d) $scCO_2$.

study previously reported [43]. Nevertheless the conformation adopted by substrate **6** on the metallic surface probably favours the hydrogenation of the double bond instead of the aromatic ring.

4. Conclusions

New Ru and Rh nanoparticles could be prepared using phosphine derivatives. Their preparation was highly dependent on the organometallic precursor and the ligand nature. While triphenylphosphine stabilised both kind of nanoparticles (**Ru3** and **Rh3**), the ligands containing fluorinated groups, **1** and **2**, were appropriate stabilisers for **Rh1** and **Ru2**, respectively. The full characterization of these materials (TEM, IR, elemental analysis and XRD) evidenced the presence of the ligands at the metallic surface. In particular, the exchange ligand reaction between **Ru2** and dodecanethiol showed the slow displacement of the phosphine **2** by the thiol derivative (monitored by NMR), pointing to a strong interaction of the ligand with the metallic surface. These nanoparticles were used as catalytic precursors in hydrogenation reactions of substrates containing aromatic groups (substrates **4**–**6**). The substrate conversions obtained show that the catalytic systems are in general slower in $scCO_2$ than in THF, probably due to the different solubilities of the MNP in $scCO_2$ than in THF even for the ligand **2** containing fluorinated groups. Ru nanoparticles remained dispersed after hydrogenation in $scCO_2$, in contrast to the agglomerates observed for RhNP. The relative higher metallic surface for Ru nanoparticles than that observed for the rhodium agglomerates agrees with the higher activity observed for Ru systems than that given for Rh ones. In addition, the selectivity observed points to a strong interaction between the phenyl groups of the substrates with the surface, mainly in the presence of oxygenated groups.

Acknowledgements

We gratefully acknowledge the financial support of the Centre National de la Recherche Scientifique, the Université Paul Sabatier, the Ministerio de Ciencia e Innovación (CTQ2007-63510PPQ and CSD2006-0003) and Generalitat de Catalunya (CTP 2007ITT-00007 and 2005SGR00777). M.V. Escárcega-Bobadilla thanks Generalitat de Catalunya and European Social Fund for a pre-doctoral fellowship (FI and BE2008).

Appendix A. Supplementary data

Supplementary data associated with this article can be found, in the online version, at doi:10.1016/j.cattod.2009.07.112.

References

[1] A. Roucoux, A. Nowicki, K. Philippot, in: D. Astruc (Ed.), Nanoparticles and Catalysis, Wiley-VCH, Weinheim, 2008 , p. 349 (Chapter 11).
[2] A. Roucoux, K. Philippot, in: J.G. de Vries, C.J. Elsevier (Eds.), The Handbook of Homogeneous Hydrogenation, Wiley-VCH, Weinheim, 2007, p. 217.
[3] D. Astruc, F. Lu, J.R. Aranzaes, Angew. Chem. Int. Ed. 44 (2005) 7852.
[4] J.A. Widegren, R.G. Finke, J. Mol. Catal. A: Chem. 191 (2003) 187.
[5] J.D. Aiken III, R.G. Finke, J. Mol. Catal. A: Chem. 145 (1999) 1.
[6] H.U. Blaser, C. Malan, B. Pugin, F. Spindler, H. Steiner, M. Studer, Adv. Synth. Catal. 345 (2003) 103.
[7] J.G. de Vries, C.J. Elsevier (Eds.), The Handbook of Homogeneous Hydrogenation, Wiley-VCH, Weinheim, 2007.
[8] K. Weissermel, H.-J. Arpe, Industrial Organic Chemistry, VCH, New York, 1993.
[9] J. Durand, E. Teuma, M. Gómez, Eur. J. Inorg. Chem. (2008) 3577.
[10] P.T. Anastas, J.C. Warner, Green Chemistry: Theory and Practice, Oxford University Press, Oxford, 1998.
[11] W. Leitner, Acc. Chem. Res 35 (2002) 746.
[12] P.G. Jessop, T. Ikariya, R. Noyori, Chem. Rev. 99 (1999) 475.
[13] A. Baiker, Chem. Rev. 99 (1999) 453.
[14] C.L. Young (Ed.), IUPAC Solubility Data Series: Hydrogen and Deuterium, vol. 5/6, Pergamon, New York, 1981.
[15] D.J. Cole-Hamilton, Science 299 (2003) 1702.
[16] F. Cansell, C. Aymonier, J. Supercrit. Fluids 47 (2009) 508.
[17] E. Reverchon, R. Adami, J. Supercrit. Fluids 37 (2006) 1.
[18] Q. Xu, W. Ni, Prog. Chem. 19 (2007) 1419.
[19] S. Moisan, V. Martinez, P. Weisbecker, F. Cansell, S. Mecking, C. Aymonier, J. Am. Chem. Soc. 129 (2007) 10602.
[20] A. Kameo, T. Yoshimura, K. Esumi, Colloids Surf. A: Physicochem. Eng. Aspects 215 (2003) 181.
[21] M.C. McLeod, R.S. McHenry, E.J. Beckman, C.B. Roberts, J. Phys. Chem. B 107 (2003) 2693.
[22] P.S. Shah, J.D. Holmes, R.C. Doty, K.P. Johnston, B.A. Korgel, J. Am. Chem. Soc. 122 (2000) 4245.
[23] P.S. Shah, S. Husain, K.P. Johnston, B.A. Korgel, J. Phys. Chem. B. 106 (2002) 12178.
[24] J.L. Zhang, B.X. Han, J. Supercrit. Fluids 47 (2009) 531.
[25] C.A. Fernandez, C.M. Wai, Small 2 (2006) 1266.

[26] J. Eastoe, S. Gold, Phys. Chem. Chem. Phys. 7 (2005) 1352.
[27] R.J. Bonilla, B.R. James, P.G. Jessop, Chem. Commun. (2000) 941.
[28] K.M.K. Yu, P. Meric, S.C. Tsang, Catal. Today 114 (2006) 428.
[29] M. Ohde, H. Ohde, C.M. Wai, ACS Symp. Ser. 860 (2003) 419.
[30] P. Meric, K.M.K. Yu, A.T.S. Kong, S.C. Tsang, J. Catal. 237 (2006) 330.
[31] M. Ohde, H. Ohde, C.M. Wai, Chem. Commun. (2002) 2388.
[32] H. Ohde, M. Ohde, C.M. Wai, Chem. Commun. (2004) 930.
[33] L.S. Ott, R.G. Finke, Coord. Chem. Rev. 251 (2007) 1075.
[34] M. Tamura, H. Fujihara, J. Am. Chem. Soc. 125 (2003) 15742.
[35] S. Jansat, M. Gómez, K. Philippot, G. Muller, E. Guiu, C. Claver, S. Castillón, B. Chaudret, J. Am. Chem. Soc. 126 (2004) 1592.
[36] M. Diéguez, O. Pàmies, Y. Mata, E. Teuma, M. Gómez, F. Ribaudo, P.W.N.M. van Leeuwen, Adv. Synth. Catal. 350 (2008) 2583.
[37] D.D. Perrin, W.L.F. Armarego, Purification of Laboratory Chemicals, 2nd ed., Pergamon Press, Oxford, 1988.
[38] K. Philippot, B. Chaudret, C. R. Chimie 6 (2003) 1019.
[39] J. Chatt, L.M. Venanzi, J. Chem. Soc. (1957) 4735.
[40] R. Usón, L.A. Oro, J. Cabeza, Inorg. Synth. 23 (1985) 126.
[41] A.T. Shulgin, A.W. Baker, J. Org. Chem. 28 (1963) 2468.
[42] B. Chaudret, Top. Organomet. Chem. 16 (2005) 233.
[43] I. Favier, S. Massou, E. Teuma, K. Philippot, B. Chaudret, M. Gómez, Chem. Commun. (2008) 3296.